1997-08-01

Modeling and simulation of crack initiation and growth in particulate composites

Kwon, Y.W.; Liu, C.T.

Journal Name: Journal of Pressure Vessel Technology; Journal Volume: 119; Journal Issue: 3; Other Information: PBD: Aug 1997
http://hdl.handle.net/10945/61022

Modeling and Simulation of Crack Initiation and Growth in Particulate Composites

Y. W. Kwon
Mem. ASME

J. H. Lee

Mechanical Engineering Department,
Naval Postgraduate School,
700 Dryer Road,
Monterey, CA 93943

C. T. Liu
Phillips Laboratory,
Edwards Air Force Base, CA 93524

A micro/macromechanical approach was used to model and simulate crack initiation and crack propagation in particulate composite structures. The approach used both the micromechanical and macromechanical analyses in tandem. The micromechanical analysis was based on a simplified micromechanical model and damage mechanics at the micro-level, and the macromechanical analysis utilized the finite element method. In using these methods, crack initiation and growth in a general shape of composite structure were investigated with an efficient computational effort. It was assumed that a crack initiates and/or propagates when localized damage is saturated. As a result, the crack length was assumed to be the size of the saturated damage zone. Matrix crack initiation and propagation at circular notch tips were simulated using this approach. Modeling and simulation were also conducted for cases of nonuniform particle distribution in particulate composite structures. Predicted results showed a good agreement with the experimental data.

Introduction

A particulate composite consists of a physical mixture of particles and a matrix material. These types of composite materials are widely used in engineering applications because of their low production costs and their significantly improved stiffness. However, the strength improvement of the particle-reinforced composites are relatively low (Johnson, 1987). As a result, it is important to understand as well as to predict the failure mechanisms and failure modes in particulate composite systems.

Possible damage modes of a particulate composite are particle/matrix debonding called dewetting, matrix damage (or cavity formation), and particle cracking. If particles are much stronger than the matrix material, failure occurs due to dewetting and/or cavity formation in the matrix material. These damages cause volume dilatation as studied by many researchers (Farris, 1968; Knauss et al., 1973; Anderson and Farris, 1988; Schapery, 1987, 1991; Ravichandran and Liu, 1995). These studies investigated the nonlinear constitutive response of a damaged particulate composite in terms of the change in volume dilatation.

Micromechanical models were considered to describe the nonlinear stress-strain behavior with damage evolution in particle-reinforced composites. Most studies included the interface debonding and/or void formation in the matrix material. In other words, the degraded effective elastic modulus of a damaged particulate composite was computed from the proposed micromechanical models (Weng, 1984; Schapery, 1986, 1991; Anderson and Farris, 1988; Tong and Ravichandran, 1994; Ravichandran and Liu, 1995). Initially, the uniaxial nonlinear stress-strain response was studied, and later it was extended to the multiaxial stress-strain response.

The objective of the present study is to develop a modeling and simulation technique to investigate damage and crack initiation and its growth until ultimate failure for particulate composite structures subject to mechanical loading. To this end, a micro/macromechanical approach was adopted. This approach utilizes both micromechanical and macromechanical analyses in tandem. A unit-cell model is used for the micromechanical analysis and the finite element analysis is utilized for the macromechanical analysis. In order to incorporate damage, the damage mechanics is applied to the unit-cell model. The detailed description of the micro/macromechanical approach is provided in the next section, which is followed by results and discussion, and conclusions.

Micro/Macromechanical Approach

The developed micro/macromechanical approach utilizes both micro-level and macro-level analyses in tandem. The micro-level analysis includes computation of stresses and strains in the constituent materials such as the particles and the binding matrix. On the other hand, the macro-level analysis performs the structural analysis of a composite. Therefore, analyses were performed at two different scales, but maintained interaction with each other. The interaction between the micromechanical and macromechanical analyses is illustrated in Fig. 1.

The macromechanical analysis utilizes the finite element method for structural analysis of a composite so that a general composite structure can be analyzed under a general loading. The micromechanical analysis adopts a simplified unit-cell model (Aboudi, 1987, 1989; Kwon, 1993; Kwon and Berner, 1994, 1995) and damage mechanics (Kachanov, 1972, 1980; Krajcinovic, 1983; Talreja, 1985). The simplified unit-cell model calculates stresses and strains in the constituent materials. Damage mechanics is applied to the micromechanical model based on the micro-level stresses and strains. Damage modes and mechanisms are described in terms of constituent materials. As a result, damage modes can be classified as matrix cracking, particle cracking, or particle/matrix interface debonding.

The interaction between the micromechanical and macromechanical analyses is explained in the forthcoming. The micromechanical analysis computes smeared composite material properties based on the constituent material properties and their damage states. This computation is conducted at every integration points of the macro-level finite element model. Thus, the macro-level finite element analysis can be undertaken as usual using the smeared composite material properties at the integration points. After the macromechanical analysis is performed, the smeared stresses and strains at the composite level are applied to the micromechanical model so that micro-level stresses

Contributed by the Pressure Vessels and Piping Division for publication in the JOURNAL OF PRESSURE VESSEL TECHNOLOGY. Manuscript received by the PVP Division, July 24, 1996; revised manuscript received April 3, 1997. Associate Technical Editor: F. Hara.

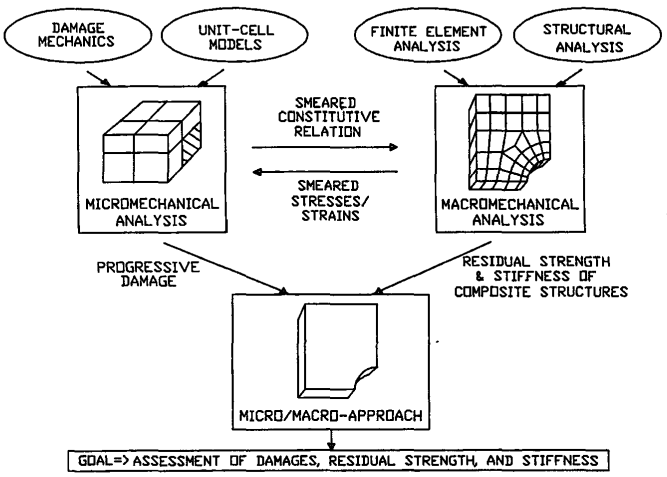

Fig. 1 Micro/macromechanical approach

and strains can be computed. This computation is also performed at the integration points. Therefore, the interaction between the micro-level analysis and the macro-level analysis occurs at the numerical integration points of the finite element model.

Using the micromechanical model, nonuniform particle distribution in a particulate composite can be easily modeled. The basis of micromechanical model and damage mechanics is presented in the forthcoming.

(a) Micromechanical Model. The micromechanical model is based on a unit-cell structure. The unit-cell consists of a particle and the surrounding matrix material, as shown in Fig. 2(*a*). A clear view of subcell locations is illustrated in Fig. 2(*b*). For a particulate composite, let subcell 1 denote the particle subcell and the rest of them be the binder matrix subcells. Planes 1-2, 2-3, and 3-1 are symmetric planes.

The micromechanical model has two objectives: one is to compute smeared composite material properties from particle and matrix material properties, respectively, under an intact or a damaged state; the other is to describe damage modes and states at the constituent material level. The development of the micromechanical model for a particulate composite is described in the forthcoming.

It is assumed that stresses/strains are uniform within each subcell for simplicity of the mathematical development. Each subcell has a constitutive equation expressed as

$$\sigma_{ij}^{\alpha} = E_{ijkl}^{\alpha}\epsilon_{kl}^{\alpha} \tag{1}$$

where the subscripts $i, j, k, l = 1, 2, 3$ denote the coordinate axes shown in Fig. 2, and α (=1 through 8) indicates a subcell. σ_{ij}^{α} and ϵ_{kl}^{α} are the average stresses and strains of the subcell α.

The unit cell stresses and strains are obtained from the volume average of the subcell stresses and strains. That is

$$\bar{\sigma}_{ij} = \sum_{\alpha=1}^{8} V^{\alpha}\sigma_{ij}^{\alpha} \tag{2}$$

$$\bar{\epsilon}_{ij} = \sum_{\alpha=1}^{8} V^{\alpha}\epsilon_{ij}^{\alpha} \tag{3}$$

Here, V^{α} is the volume fraction of the αth subcell, and $\bar{\sigma}_{ij}$ and $\bar{\epsilon}_{ij}$ are the average unit-cell stresses and strains, respectively. These are the effective stresses and strains of a composite.

One of the objectives of the micromechanical model is to find the relation between the unit-cell stresses and strains (i.e., the constitutive relation at the composite level) using the material informations at the subcell level. To this end, stress and strain compatibility equations are applied. First of all, the stress equilibrium at each subcell interface is

$$\sigma_{11}^{1} = \sigma_{11}^{2}, \quad \sigma_{11}^{3} = \sigma_{11}^{4}, \quad \sigma_{11}^{5} = \sigma_{11}^{6}, \quad \sigma_{11}^{7} = \sigma_{11}^{8} \tag{4}$$

$$\sigma_{22}^{1} = \sigma_{22}^{3}, \quad \sigma_{22}^{2} = \sigma_{22}^{4}, \quad \sigma_{22}^{5} = \sigma_{22}^{7}, \quad \sigma_{22}^{6} = \sigma_{22}^{8} \tag{5}$$

$$\sigma_{33}^{1} = \sigma_{33}^{5}, \quad \sigma_{33}^{2} = \sigma_{33}^{6}, \quad \sigma_{33}^{3} = \sigma_{33}^{7}, \quad \sigma_{33}^{4} = \sigma_{33}^{8} \tag{6}$$

Only normal stress components are shown in these equations. Similar equations can be written for shearing stress components. However, it is assumed that each subcell material is orthotropic or isotropic so that normal stress/strain components are not coupled with shear components. Thus, the present development is only for the normal components of stresses/strains and a similar development can be made for shearing stresses/strains.

Strain compatibility is assumed to be

$$l_p\epsilon_{11}^{1} + l_m\epsilon_{11}^{2} = l_p\epsilon_{11}^{3} + l_m\epsilon_{11}^{4} = l_p\epsilon_{11}^{5} + l_m\epsilon_{11}^{6} = l_p\epsilon_{11}^{7} + l_m\epsilon_{11}^{8} \tag{7}$$

$$l_p\epsilon_{22}^{1} + l_m\epsilon_{22}^{3} = l_p\epsilon_{22}^{2} + l_m\epsilon_{22}^{4} = l_p\epsilon_{22}^{5} + l_m\epsilon_{22}^{7} = l_p\epsilon_{22}^{6} + l_m\epsilon_{22}^{8} \tag{8}$$

$$l_p\epsilon_{33}^{1} + l_m\epsilon_{33}^{5} = l_p\epsilon_{33}^{2} + l_m\epsilon_{33}^{6} = l_p\epsilon_{33}^{3} + l_m\epsilon_{33}^{7} = l_p\epsilon_{33}^{4} + l_m\epsilon_{33}^{8} \tag{9}$$

in which

$$l_p = V_p^{1/3} \tag{10}$$

$$l_m = 1 - l_p \tag{11}$$

and V_p is the particle volume fraction of a composite.

Substitution of Eq. (1) into Eqs. (4) through (6) yields the stress compatibility equations in terms of subcell strains. For example, one of Eq. (4) becomes

$$E_{11kl}^{1}\epsilon_{kl}^{1} = E_{11kl}^{2}\epsilon_{kl}^{2} \tag{12}$$

Similar expressions hold for the rest of equations in Eqs. (4) through (6). These equations along with Eqs. (3), (7), (8), and (9) can relate the subcell strains to unit-cell strains. That is

$$[A]\{\epsilon\} = \{\bar{\epsilon}\} \tag{13}$$

in which $\{\epsilon\}$ is the vector consisting of subcell strains ϵ_{ij}^{α}, while $\{\bar{\epsilon}\}$ is the vector consisting of the unit-cell strains $\bar{\epsilon}_{ij}$ and zero. In addition, $[A]$ is the matrix containing material properties and geometric properties of the subcells like E_{ijkl}^{α}, V^{α}, l_p, and l_m.

Matrix $[A]$ is invertible so that solving Eq. (13) results in the expression for the unit-cell strains in terms of subcell strains. That is

$$\{\epsilon\} = [A]^{-1}\{\bar{\epsilon}\} \tag{14}$$

Equation (14) gives the explicit relationship between the subcell and unit-cell strains (i.e., strains at the constituent level like the particle and the matrix, and strains at the composite level).

Finally, in order to determine the constitutive relation between the unit-cell stresses and strains, Eq. (1) is substituted into Eq. (2). This operation yields the expression for the unit-cell stresses in terms of subcell strains. The subcell strains are replaced by unit-cell strains using Eq. (14), Then, the unit-cell

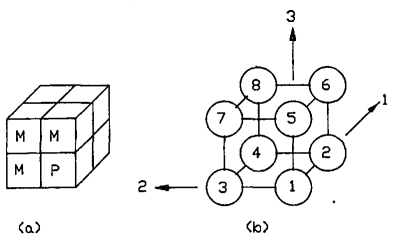

Fig. 2 Micromechanical unit-cell model

stresses are directly related to the unit-cell strains. The relating constitutive expression is given in terms of the material and geometric properties of the subcells. In other words, the composite level constititive equation is expressed in terms of the particle and matrix properties like

$$\bar{\sigma}_{ij} = \bar{E}_{ijkl}\bar{\epsilon}_{kl} \tag{15}$$

where $\bar{E}_{ijkl}$ is the constitutive relation of the composite.

(b) Damage Mechanics. Damage mechanics is applied to the constituent materials like the particles and matrices in order to predict the damage initiation and evolution until failure. Therefore, damage modes can be described in a fundamental way such as matrix cracking, particle cracking, and particle/matrix interface debonding.

Let us consider one constituent material, the matrix for example, for the development of the damage theory. From now on, vector and matrix notations will be adopted instead of tensor notations for simplicity. Thus, stresses and strains are expressed in vector format. The strain increment in the material may be written as

$$\{d\epsilon\} = \{d\epsilon\}_v + \{d\epsilon\}_d \tag{16}$$

where $\{d\epsilon\}$ is the total strain increment, and subscripts v and d denote the virgin and damaged states, respectively. In other words, the total strain increment consists of the strain increment without damage and the strain increment due to damage.

The constitutive equation for the virgin material is

$$\{d\sigma\} = [E]_v\{d\epsilon\}_v \tag{17}$$

while the incremental strain due to the damage is assumed to be expressed as

$$\{d\epsilon\}_d = d\lambda \frac{\partial F_d}{\partial\{\sigma\}} \tag{18}$$

in which F_d is the damage potential function. The damage potential function varies depending on the amount of damage state. Thus, it can be assumed that

$$F_d = F_d(\{\sigma\}, \{\epsilon\}_d) \tag{19}$$

If the damage potential function is also used for the damage criterion, the damage state must satisfy $F_d = 0$. As a result, Eq. (19) can be written as

$$dF_d = \left\{\frac{\partial F_d}{\partial\{\sigma\}}\right\}^T\{d\sigma\} + \left\{\frac{\partial F_d}{\partial\{\epsilon\}_d}\right\}^T\{d\epsilon\}_d = 0 \tag{20}$$

Using Eqs. (16), (17), and (20) yields

$$d\lambda = \frac{\{Q\}^T[E]_v\{d\epsilon\}}{\{R\}^T\{Q\} + \{Q\}^T[E]_v\{Q\}} \tag{21}$$

where

$$\{Q\} = \left\{\frac{\partial F_d}{\partial\{\sigma\}}\right\} \tag{22}$$

and

$$\{R\} = \left\{\frac{\partial F_d}{\partial\{\epsilon\}_d}\right\} \tag{23}$$

Substitution of Eq. (21) into Eq. (18), and combining the resultant equation with Eqs. (16) and (17), gives

$$\{d\sigma\} = [E]_d\{d\epsilon\} \tag{24}$$

in which the constitutive matrix for the damaged material is

$$[E]_d = [E]_v\left([I] - \frac{\{Q\}\{Q\}^T[E]_v}{\{R\}^T\{Q\} + \{Q\}^T[E]_v\{Q\}}\right) \tag{25}$$

The damage potential function is dependent on the constituent material and can be rewritten as

$$F_d = f(\{\sigma\}) - g((\epsilon_d)_e) \tag{26}$$

in which f and g are assumed to be

$$f = (J_2')^{1/2} \tag{27}$$

and

$$g = \sigma_d + a_1 \tanh(a_2(\epsilon_d)_e) \tag{28}$$

Here, σ_d is the damage initiation strength of the material, $(\epsilon_d)_e$ is the effective damage strain, and a_1 and a_2 are the material constants. The material properties are determined from the uniaxial stress-strain curve. Function g is dependent on the damage state.

In the present study, the damage mechanics is applied only to the matrix material, but not to the particle material because the particles are much stiffer and stronger than the matrix in the present composite. In the micro/macromechanical approach, the micromechanical model represents average stresses/strains around each numerical integration point of an isoparametric finite element. As a result, the representing area by the micromodel depends on the size of finite elements and the number of integration points for each element. When smaller elements and more integration points are used in the finite element analysis, the area represented by the micromechanical model will be smaller and more accurate. However, a compromise must be made between the accuracy and the computational cost. Then, damage mechanics is applied to the matrix subcells of the micromodel at each numerical integration point when the subcell stresses exceed the threshold damage strength.

Results and Discussion

The study considered particulate composite specimens consisting of hard particles bound by a soft matrix material. Thus, matrix crack initiation and crack propagation were predicted using the developed micro/macromechanical approach. The analysis simulated matrix damage initiation and damage propagation in particulate composites using the micromechanical model and damage mechanics as described in the previous section. When the damage was saturated in a local zone, the location could not sustain any additional loading. Thus, it was assumed that a crack occurred within the saturated damage zone. That is, the crack length was equal to the size of the saturated damage zone.

Hercules particulate composites were used in this study. The typical stress-strain curve of the particulate composite is provided in Fig. 3. This curve is the macro-level smeared material property. The micromechanical model requires the material properties of the constituent materials and their volume fractions. However, this information was not known. Therefore, it was necessary to back-calculate the micro-level material properties from the macro-level material properties using the proposed micromechanical model and the damage mechanics. The computed micro-level material properties were as follows. The particle elastic modulus was 10×10^6 psi, the matrix modulus was 335 psi, and the particle volume fraction was 0.65. In addition, the damage initiation strength of the matrix material in Eq. (28) was 70 psi, and the damage material constants were $a_1 = 92$ psi and $a_2 = 12$. The reproduced stress-strain curve using the micromechanical and damage model and these material constants is also shown in Fig. 3. The experimental curve agreed well with the predicted curve. By this, the micro-level material values were assumed to be correct.

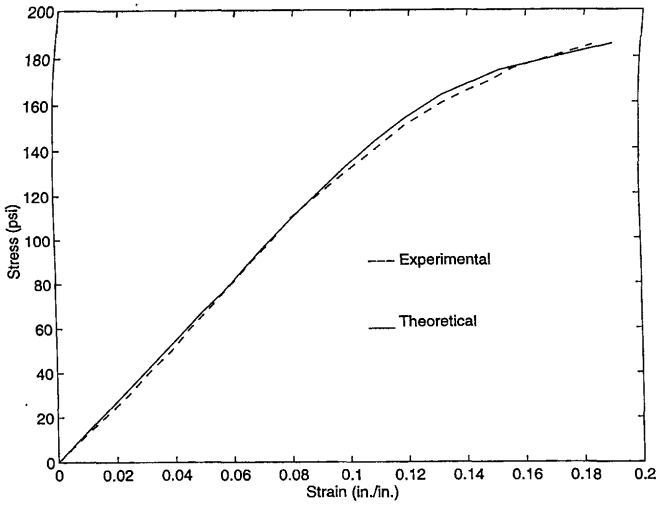

Fig. 3 Stress-strain curve

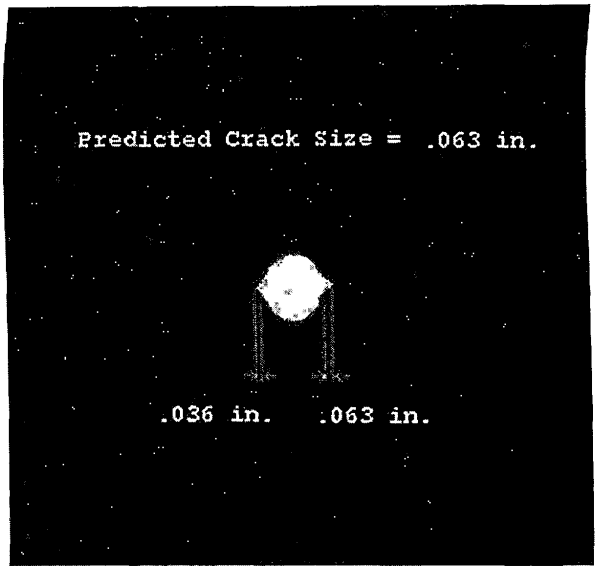

Fig. 5 Composite specimen with a 0.25-in. hole

The same material was tested with a hole at the center. Tensile loads were applied to the specimens with constant cross-head speed of 5.08 mm/min (0.2 in./min). Cracks initiated from stress concentration at the edges of the holes. Figures 4–5 show the cracks in the specimens at strain of 0.2 m/m. One specimen had 6.35-mm- (0.25-in-) dia hole, while the other specimen had 12.7-mm- (0.5-in-) dia hole. Both specimens resulted in quite asymmetric cracks at both sides of the holes.

These test results can be explained from nonhomogeneity of particle distribution in the matrix material. As observed from the tensile test of a dogbone-shape specimen without a hole, the local strain was very different from location to location within the specimen under the constant load. This nonuniform strain was believed to have resulted from the nonuniform particle distribution. The experimental stress-strain curve in Fig. 3 used the average strain between the gage length of 68.58 mm (2.7 in.).

When a hole is drilled into the specimen, the hole may lie in a particle-dense zone or a particle-sparse zone of the specimen, even though the overall stress-strain curve remains constant. Because the specimen was under strain control, the local strain and stress were different around the hole depending on its location. As a result, the crack size varied depending on the location of the hole in the specimen. Asymmetric cracks at both sides of the hole might be caused by various factors including, but not limited to, asymmetric hole shape and location, asymmetric particle distribution, and/or misaligned loading.

Computer simulation was conducted to predict the cracks observed in the experiment. A finite element mesh for the specimen with a 6.35-mm (0.25-in.) hole is shown in Fig. 6. Because of symmetry, a quarter of the specimen was modeled. First of all, it was assumed that the specimen had a uniform material property, i.e., uniform particle distribution. The specimen with a 12.7-mm- (0.5-in-) dia hole was considered first. The predicted crack size is also shown in Fig. 4 along with the actual cracks in the experiment. The predicted crack length was 3.175 mm (0.125 in.), while the physical cracks were 2.03 mm (0.08 in.) and 3.81 mm (0.15 in.) at both sides of the specimen. Therefore, the predicted crack size agreed well with the experimental crack.

When the other specimen with a 6.35-mm- (0.25-in-) dia hole was modeled with a uniform particle distribution, the predicted crack length was much larger than the experimental crack length. The next simulation assumed that the lower half of the specimen in Fig. 6 had a different particle volume fraction (PVF) from the upper half of the specimen. However, the average stress-strain curve also matched with the experimental curve, as given in Fig. 3. Two cases were studied. The first

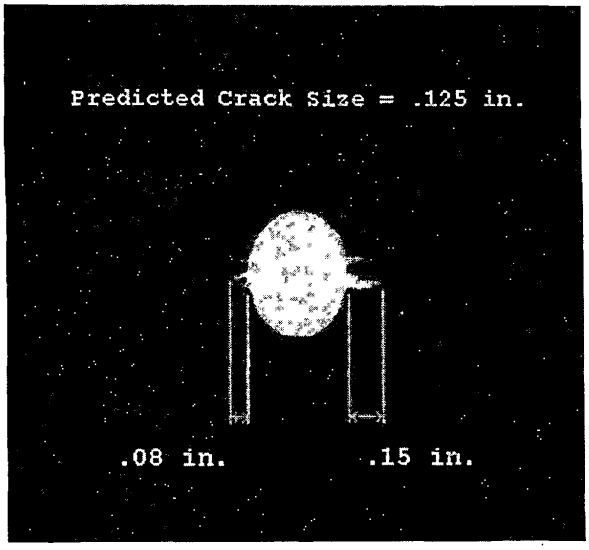

Fig. 4 Composite specimen with a 0.5-in. hole

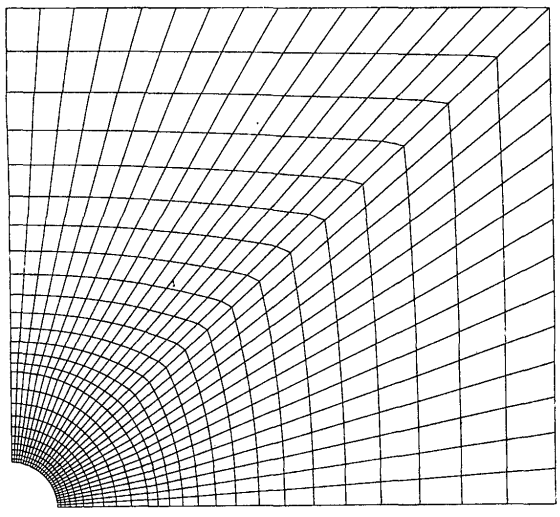

Fig. 6 Finite element mesh with a 0.25-in. hole

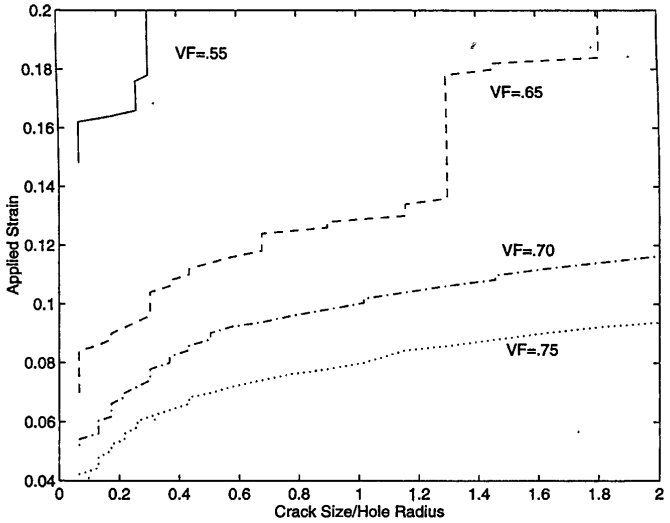

Fig. 7 Normalized crack size versus applied uniform strain for different particle volume fractions

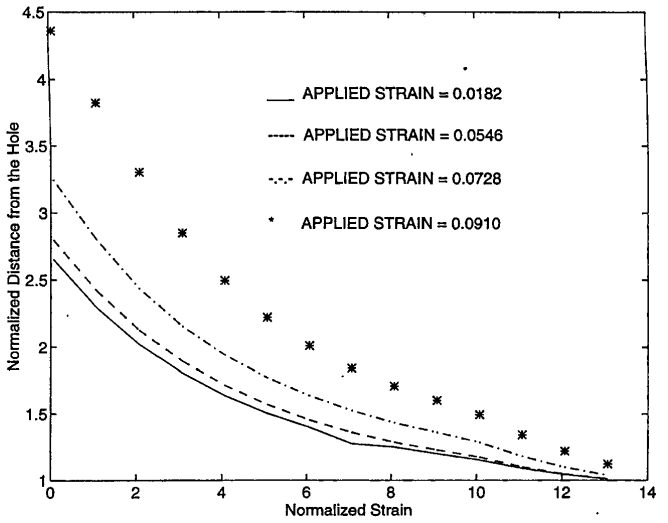

Fig. 9 Normalized strain versus displacement plots under various strain-controlled loads

case considered the lower half of the specimen at a PVF of 55 percent, while the upper half at 75 percent. Thus, the zone including the hole had a PVF of 55 percent. The other case had opposite volume fractions so that the hole was placed at the particle-dense zone. The first case with a hole at the particle-sparse zone predicted a crack size of 1.60 mm (0.063 in.), which was close to the experimental cracks of 1.60 mm (0.063 in.) at one side of the hole and 0.91 mm (0.036 in.) at the other side of the hole. On the other hand, the second case resulted in a crack length of 11.68 mm (0.460 in.). Therefore, the small crack at the second specimen was possibly caused by the location of the hole at the particle-sparse zone.

Parametric studies were undertaken next to investigate the crack initiation and propagation under two different loading conditions: uniform strain (displacement) and uniform traction loading conditions. Different PVFs were considered in both studies. The particle distribution was assumed to be uniform across the specimen with a 6.35-mm (0.25-in.) center hole. Crack size versus applied strain is shown in Fig. 7 for different PVFs, while crack size versus applied traction is shown in Fig. 8. Both results showed a stable crack growth from the notch tip.

The displacement-controlled loading resulted in several temporary crack stops before the crack grew further; that is, the crack did not propagate at certain lengths until there was a jump in the applied strain. This indicates the crack blunting process. The stairs-shape graphs in Fig. 7 illustrate the temporary crack arrest process, which was also observed in the experimental study. The crack arrest was more significant for a lower PVF. As expected, a higher PVF yielded a larger crack size under the same applied strain.

For the load-controlled specimen, the results indicated that the crack size increased continuously at almost the same rate as the applied load regardless of PVF. Under the load control, the stress state was so similar that there was not much difference in the crack size among various PVFs. A higher PVF yielded a lower stress in the matrix because the particles supported a larger portion of the load. Hence, a higher PVF yielded a smaller crack size under the same load. However, the difference was much less than that under the displacement control.

Figure 9 shows the normalized strain distributions at the minimum cross section of the specimen. The specimen had a hole diameter of 12.7 mm (0.5 in.) with PVF = 0.65. In the figure, the strain was normalized with respect to the applied uniform strain at the ends of the specimen, while the distance was normalized in terms of the hole radius. The graph with the applied strain at 0.0182 shows the strain distribution before damage occurs in the matrix material. However, as the damage progressed and a crack initiated with an increased strain loading, the normalized strain further increased near the notch tip; the damaged or cracked matrix material could not support the load any more.

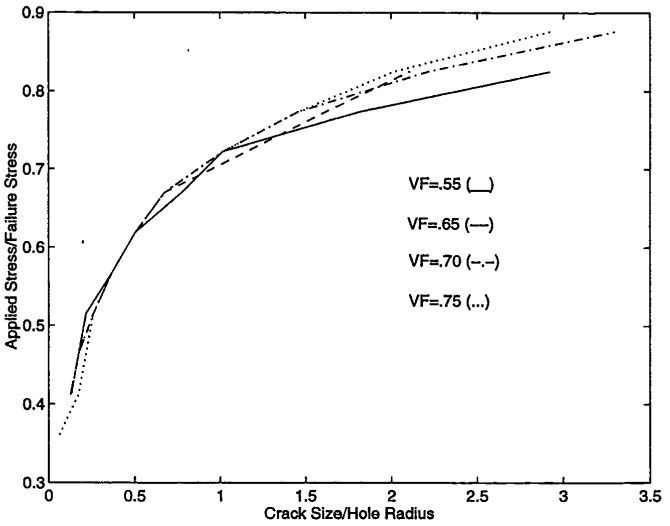

Fig. 8 Normalized crack size versus applied uniform stress for different particle volume fractions

Conclusions

A micro/macromechanical approach was developed to model and simulate crack initiation and propagation in particulate composites. The approach was based on a simplified micromechanical model, damage mechanics at the micro-level, and the finite element analysis at the macro-level. Both micromechanical and macromechanical analyses were conducted in tandem. The micro/macromechanical approach could be applied to a general particulate composite structure, and it was also computationally efficient.

The proposed approach could predict matrix cracks in particulate composite specimens accurately. Furthermore, the micro/macromechanical approach could easily model nonuniform particle distributions in particulate composites because most particulate composites showed nonuniform particle distributions. The prediction with nonuniform particle distributions showed good comparison with experimental results.

Further analysis indicated that the displacement control of tensile specimens resulted in a smaller crack size for a smaller PVF subjected to the same global strain. On the other hand, the load-controlled specimens yielded the opposite results. However, the displacement-controlled specimens produced a much larger difference among different PVFs than the load-controlled specimens.

References

Aboudi, J., 1987, "Closed Form Constitutive Equations for Metal Matrix Composites," *International Journal of Engineering Science,* Vol. 25, pp. 1229–1240.

Aboudi, J., 1989, "Micromechanical Analysis of Composites by the Method of Cells," *Applied Mechanics Review,* Vol. 42, pp. 193–221.

Anderson, L. L., and Farris, R. J., 1988, "A Predictive Model for the Mechanical Behavior of Particulate Composites," *Journal of Polymer Engineering Science,* Vol. 28, pp. 522–528.

Farris, R. J., 1968, "The Character of the Stress-Strain Function for Highly Filled Elastomers," *Trans. Society of Rheology,* Vol. 12, pp. 303–314.

Johnson, W. S., 1987, "Metal Matrix Composites. Their Time to Shine?," *ASTM Standardization News,* Oct., pp. 36–39.

Kachanov, M., 1972, "On the Continuum Theory of Medium With Cracks," *Mechanics of Solids,* Vol. 7, (2), pp. 50–54.

Kachanov, M., 1980, "Continuum Model of Medium With Cracks," *ASCE Journal of Engineering Mechanics Division,* Vol. 106 (EM5), pp. 1039–1051.

Knauss, W. G., Palaniswamy, and Smith, G. C., 1973, "The Application of Rate Theory to the Failure of Solid Propellants," GALCIT SM Report 73-3, California Institute of Technology, Pasadena, CA.

Krajcinovic, D., 1983, "Constitutive Equations for Damaging Materials," ASME *Journal of Applied Mechanics,* Vol. 50, pp. 355–360.

Kwon, Y. W., 1993, "Calculation of Effective Moduli of Fibrous Composites With or Without Damages," *Composite Structures,* Vol. 25, pp. 187–192.

Kwon, Y. W., and Berner, J. M., 1994, "Analysis of Matrix Damage Evolution in Laminated Composite Plates," *Engineering Fracture Mechanics,* Vol. 48 (6), pp. 811–817.

Kwon, Y. W. and Berner, J. M., 1995, "Micromechanics Model for Damage and Failure Analyses of Laminated Fibrous Composites," *Engineering Fracture Mechanics,* Vol. 52 (2), pp. 231–242.

Ravichandran, G., and Liu, C. T., 1995, "Modeling Constitutive Behavior of Particulate Composites Undergoing Damage," *International Journal of Solids Structures,* Vol. 32, No. 6/7, pp. 979–990.

Schapery, R. A., 1986, "A Micromechanical Model for Non-linear Viscoelastic Behavior of Particle-Reinforced Rubber With Distributed Damage," *Engineering of Fracture Mechanics,* Vol. 25, pp. 845–867.

Schapery, R. A., 1987, "Deformation and Fracture of Inelastic Composite Materials Using Potential," *Journal of Polymer Engineering Science,* Vol. 27, pp. 63–76.

Schapery, R. A., 1991, "Analysis of Damage Growth in Particulate Composites Using a Work Potential," *Composite Engineering,* Vol. 1, pp. 167–182.

Talreja, R., 1985, "A Continuum Mechanics Characterization of Damage in Composite Materials," *Proceedings of Royal Society of London,* Vol. A399, pp. 195–216.

Tong, W., and Ravichandran, G., 1994, "Effective Elastic Moduli and Characterization of a Particle-Reinforced Metal Matrix Composite With Damaged Particles," *Computer Science Technology,* Vol. 52, pp. 247–252.

Weng, G. J., 1984, "Some Elastic Properties of Reinforced Solids, With Special Reference to Isotropic Ones Containing Spherical Inclusions," *International Journal of Engineering Science,* Vol. 22, pp. 845–856.

Transactions of the ASME

Technical Editor, S. Y. ŽAMRIK
Past Technical Editors
I. BERMAN
R. E. NICKELL
R. H. GALLAGHER
G. E. O. WIDERA
Associate Technical Editors
S. K. BHANDARI (1999)
S. S. CHEN (1999)
F. HARA (1999)
R. SESHADRI (1999)
R. SWINDEMAN (1999)
E. TENCKHOFF (1999)
Computer Technology
G. HULBERT (1999)
Design & Analysis
M. B. RUGGLES (1999)
Fluid Structure Interaction
Y. W. KWON (1999)
Materials & Fabrication
J. A. TODD (1999)
Operations, Applications & Components
I. T. KISISEL (1999)
Seismic Engineering
T. H. LIU (1999)
NDE Engineering Division
J. C. DUKE, Jr. (1999)
Pressure Vessel Research Council
M. PRAGER (1999)

BOARD ON COMMUNICATIONS
Chairman and Vice-President
R. MATES

OFFICERS OF THE ASME
President, KIETH THAYER
Executive Director, D. L. BELDEN
Treasurer, J. A. MASON

PUBLISHING STAFF
Managing Director, Engineering
CHARLES W. BEARDSLEY
Director, Technical Publishing
PHILIP DI VIETRO
Managing Editor, Technical Publishing
CYNTHIA B. CLARK
Managing Editor, Transactions
CORNELIA MONAHAN
Production Coordinator
LYNN ROSENFELD
Production Assistant
MARISOL ANDINO

Transactions of the ASME, Journal of Pressure Vessel Technology (ISSN 0094-9930) is published quarterly (Feb., May, Aug., Nov.) for $185.00 per year by The American Society of Mechanical Engineers, 345 East 47th Street, New York, NY 10017. Periodicals postage paid at New York, NY and additional mailing offices. POSTMASTER: Send address changes to Transactions of the ASME, Journal of Pressure Vessel Technology, c/o THE AMERICAN SOCIETY OF MECHANICAL ENGINEERS, 22 Law Drive, Box 2300, Fairfield, NJ 07007-2300.
CHANGES OF ADDRESS must be received at Society headquarters seven weeks before they are to be effective. Please send old label and new address. PRICES: To members, $40.00, annually: to nonmembers, $185.00. Add $30.00 for postage to countries outside the United States and Canada.
STATEMENT from By-Laws. The Society shall not be responsible for statements or opinions advanced in papers or . . . printed in its publications (B7.1, Par. 3). COPYRIGHT © 1997 by The American Society of Mechanical Engineers. Authorization to photocopy material for internal or personal use under circumstances not falling within the fair use provisions of the Copyright Act is granted by ASME to libraries and other users registered with the Copyright Clearance Center (CCC). Transactional Reporting Service provided that the base fee of $3.00 per article is paid directly to CCC, Inc., 222 Rosewood Drive, Danvers, MA 01923. Request for special permission or bulk copying should be addressed to Reprints/Permission Department. INDEXED by Applied Mechanics Reviews and Engineering Information, Inc. Canadian Goods & Services Tax Registration #126148048.

Journal of Pressure Vessel Technology

Published Quarterly by The American Society of Mechanical Engineers

VOLUME 119 • NUMBER 3 • AUGUST 1997

Announcements and Special Notices